Heliyon 10 (2024) e40513

Contents lists available at ScienceDirect

Heliyon

journal homepage: www.cell.com/heliyon

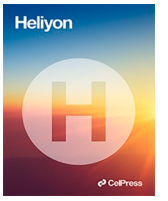

Research article

The effect of capping agent on morphology, surface functionalization, and bio-compatibility properties of $KTiOPO_4$ nanoparticles

Elaheh Gharibshahian [a,b,*], Maliheh Gharibshahian [c,d], Majid Jafar Tafreshi [b], Marjan Bahraminasab [c,d], Samaneh Arab [d]

[a] Department of Physics, National University of Skills (NUS), Tehran, Iran
[b] Faculty of Physics, Semnan University, Semnan, Iran
[c] Nervous System Stem Cells Research Center, Semnan University of Medical Sciences, Semnan, Iran
[d] Department of Tissue Engineering and Applied Cell Sciences, School of Medicine, Semnan University of Medical Sciences, Semnan, Iran

ARTICLE INFO

Keywords:
Potassium titanyl phosphate
Biocompatibility
Capping agent
Shape control
Glycine
Oxalic acid

ABSTRACT

$KTiOPO_4$ (KTP) nanoparticles (NPs) are potential materials as biolabels for long-term imaging. Optimizing their properties can lead to higher imaging efficiency and lower cytotoxicity and side effects. In this study, these nanoparticles were synthesized using the co-precipitation method and capping agents of oxalic acid and glycine. The capping agent's effect on the structural, optical, morphological, hemocompatibility, and biocompatibility properties of the obtained nanoparticles was studied. The smallest (12.56 nm) grain size and the lowest lattice strain (0.0024) were obtained using 1:1 and 1:3 mol ratios of glycine, respectively. Oxalic acid as a capping agent resulted in needle-type, flower-type, and oval-form NPs. Polygonal tablet form, cubic, and polyhedral forms of KTP NPs were synthesized using glycine. C–O–H bending bonds, O–H, N–H, and carbonyl (C=O) stretching bonds remain on the surface of synthesized NPs after heat treatment and functionalization of their surface. Our results showed that the surface functionalization modifies the biocompatibility properties of NPs. The 1:3 mol ratio of oxalic acid as a capping agent resulted in the perfect KTP NPs for long-term imaging studies. The presence of hydroxyl groups improved the biocompatibility of obtained KTP NPs using a 1:3 mol ratio of oxalic acid over time. The needle form of obtained NPs resulted in an increase in cell cytotoxicity at higher concentrations.

1. Introduction

The biological information on temporal and spatial scales is investigated using Molecular imaging [1]. This method is an essential tool for monitoring invivo response and assessing outcomes in targeted therapies [2]. Nowadays, fluorescence microscopy is a conventional technique for molecular imaging of cells, tissues, and living organs. However, due to the photobleaching phenomenon, the recording time in the biological environment is limited and can even induce phototoxicity.

Photostability and non-blinking behavior are needed for long-term cellular imaging. The far off-resonance excitation of inorganic

* Corresponding author. Department of Physics, National University of Skills (NUS), P.O.Box:1435761137, Tehran, Iran.
E-mail address: gharibshahian.e@gmail.com (E. Gharibshahian).

https://doi.org/10.1016/j.heliyon.2024.e40513
Received 25 July 2024; Received in revised form 26 October 2024; Accepted 18 November 2024
Available online 22 November 2024

Table 1
Characteristic properties of obtained KTP NPs.

sample	Lattice strain (Ɛ)	Grain size (nm)	Grain size (nm)	Crystal lattice constant			Card number	Particle size (nm)	Polydispersity index (PDI)
		William-Son	Scherer	a	B	c			
Gl1:1	0.0083	24.70	12.56	12.81	10.61	6.40	2073-070-01	55	1.05
Gl1:2	0.0031	57.75	48.67	12.81	10.61	6.40	2073-070-01	95	1.15
Gl1:3	0.0024	60.26	65.06	12.81	10.61	6.40	2073-070-01	110	1.19
OX1:1	0.0039	49.70	44.42	12.81	10.61	6.40	2073-070-01	65	1.14
OX1:2	0.0046	67.00	52.32	10.58	12.81	6.40	0802-35-00	297	1.11
OX1:3	0.0027	69.94	54.46	10.58	12.81	6.40	0802-35-00	92	1.23
Without capping agent	0.0010	50.00	50.00	10.58	12.81	6.40	0802-35-00	100	1.265

nanocrystalline results in perfect photostability and makes these crystals suitable for long-term imaging.

Satisfactory properties of KTP nanocrystalline, such as the photostable and blinking-free manner of second harmonic generation (SHG) beams, are reported by Xuan et al. [3]. These properties make KTP NPs an appropriate and attractive choice as a bio-label [4] and a vital element in SHG microscope structure [5]. Attractive properties of KTP material, such as high nonlinear optical, thermally stable phase-matching, high optical damage threshold, large linear electro-optic, and low dielectric constants, make it interesting and suitable for second harmonic generation in lasers and various electro-optical applications in both nano and bulk dimensions [5–7].

The properties of NPs depend on their shape and size. The size and shape of NPs are strongly affected by synthesis conditions such as solution pH, concentration, temperature, and applied rotation rate. Using various ligands to determine the surface energy of nuclei is one of the effective methods [8] to control the nucleation and growth of NPs and their optimization. The growth rates in different crystal directions can be tailored by modulating the relative surface energies of crystal faces using selective surface ligands [9].

Different methods, such as Pechini [10], Sol-gel [11], Mechanochemical mixing [12], Combustion [13], Co-precipitation [14,15], and hydrothermal [16] have been used to synthesize KTP nanostructures. Co-precipitation is an appropriate, cheap, and simple method for controlling the size and shape of NPs [14,15,17]. In this method, capping agents with selective adsorption to specific crystal faces can be used to kinetically control the single-crystalline growth. Also, it plays a vital role in the formation of nanocrystal morphology. By controlling the relative rate of nucleation and growth during the NPs synthesis process, shape, size, and size distribution will be controlled [18].

Oxalic acid, due to its resonance bands and small size, has a bioconjugation role between the primary nuclei and can produce well-coated nuclei and directional growth of NPs [15,19]. Stabilization of NPs using bio-capping agents, such as amino acids and oxalic acid [19,20], because of low biological toxicity is attractive for bio-related applications such as drug delivery, imaging, and cosmetics [21,22]. Amino acids act as an agglomeration controller and shape modifier when used as a capping agent [20]. Glycine, a natural amino acid, has been used as the bio-capping agent, which becomes amphoteric in an aqueous medium. This amino acid can influence the structural, morphological, and optical properties of NPs [22]. Mayer et al. [4] reported the synthesis of KTP NPs for bio-imaging applications. However, the effect of shape, surface functionalization, and concentration of KTP NPs on their biocompatibility properties isn't reported.

This paper reported the synthesis of KTP NPs by the co-precipitation method. Oxalic acid and glycine were selected as capping agents to control the size and shape of NPs and their surface functionalization. Different concentrations of capping agents (1:1, 1:2, and 1:3) were adopted. The effect of type and concentration of capping agent on structural, morphological, optical, hemocompatibility, and bio-compatibility properties of obtained NPs were studied. The effect of surface functionalization and the shape of KTP NPs on their biocompatibility were investigated. Finally, the best capping agent and the optimum concentration to produce perfect KTP NPs for long-term imaging applications were introduced.

2. Materials and methods

2.1. Synthesis method

The raw materials used for KTP NPs synthesize are as follows.

(a) Freshly $Ti(OH)_4$ powders, (b)Potassium dihydrogen phosphate (KH_2PO_4), (c)Potassium carbonate (K_2CO_3), (d) HCl (35 %), (e) Oxalic acid and Glycine as capping agents with high purity.

To produce KTP NPs, the aqueous titanyl chloride solution (which was produced by dissolving $Ti(OH)_4$ powders in HCl (6 N) solution) was mixed well with the selected capping agent in different mole ratios to titanium ion (1:1, 1:2, and 1:3). Then, an aqueous solution of potassium dihydrogen phosphate (with o.5 M concentration) was added dropwise to the capping agent-mixed titanyl

chloride solution. The potassium carbonate was used to adjust the solution pH. The white precipitate was obtained at pH ~ 6. The precipitate was washed with distilled water several times to remove chloride ions from the solid and dried at 100 °C under ambient conditions. Calcination at 700 °C for 2h was done to produce nanocrystalline powders of KTP and to remove the organic residues of capping agents. Structural properties, Polydispersity index (PDI), and particle size for all samples are given in Table 1.

2.2. Characterization

2.2.1. Physical characterization of KTP NPs

The synthesized KTP NPs were characterized by X-ray powder diffraction (XRD) using an Advanced Bruker D8 X-ray diffractometer with CuKα radiation ($\lambda = 1.5405$ Å) at a scan rate of 0.065°min^{-1}. The structural phase, the grain size, and the lattice strain of produced KTP NPs were calculated using recorded XRD spectra [23,24]. The formation of the KTP structure and its characteristic bonds was investigated by recorded Fourier transform infrared (FTIR) spectra. The KBr pellet technique was used to scan samples. Spectra were recorded on an 8400S- SHIMADZU infrared spectrometer. Raman spectrometer (Almega Thermo Nicolet Dispersive Raman spectrophotometer, Germany) in the range of 0–1000 cm^{-1} was used to evaluate the structural changes of NPs. Optical properties of obtained NPs, such as optical transparency, optical quality, cut-off wavelength, and band gap energy, were studied using UV–Vis transmission spectra. The UV-1601 Shimadzu visible spectrometer in the spectral region 200–800 nm was used to record the UV–Vis spectra of samples. The colloidal solution of KTP in ethanol was used for UV–Vis analysis. The morphology of nanostructures and their elemental distribution were observed by HITACHI S4160 scanning electron microscope (SEM) equipped with energy dispersive x-ray spectroscopy (EDX). Samples were sputtered on a copper substrate and then coated with gold-palladium to make them conductive before SEM analysis [25].

2.2.2. Cell culture

The human LAN-5 neuroblastoma cell line was cultured in RPMI 1640 culture media (Gibco, Grand Island, USA) containing 10 % of fetal bovine serum (FBS) (Gibco, Grand Island, USA), 100 units/ml of penicillin (Gibco, Grand Island, USA), and 100 μg/ml of streptomycin (Gibco, Grand Island, USA) at 37 °C in a humidified atmosphere of 95 % air and 5 % CO_2 unless otherwise indicated.

2.2.3. MTT assay

Cell viability was evaluated using an MTT assay kit (Sigma-Aldrich). Briefly, the LAN-5 cell line was seeded at 5×10^4 cells/well in 96-well plates and incubated at 37 °C in a humidified atmosphere of 95 % air and 5 % CO_2 (24h). Specific amounts of nanoparticles were dissolved in serum-free media and serially diluted after filtering (6.25, 12.5, 25, 50, and 100 μg/ml). The cells were exposed to different concentrations of NPs and then incubated for 24 and 48h. In the next step, the MTT solution was added to each well and incubated for 4h (37 °C). In this step, the formed formazan crystals were dissolved in 100 μL acid/alcohol (0.04NHCl in isopropanol) by mixing. A microplate reader was used to determine the optical density of samples (570 nm). Cell viability was calculated based on Equation (1) and the absorption rate of samples (ODn) and blank (ODb).

$$\text{Cell viability} = \frac{100 \times \text{ODn}}{\text{ODb}} \tag{1}$$

2.2.4. Lactate dehydrogenase (LDH) assay

A cytotoxicity detection kit containing lactate dehydrogenase (LDH) was used to analyze cytotoxicity activity (Roche Applied Science, Germany). First, 10^4 LAN-5 cell line was cultured in 96-well plates (24 h) and then exposed to different concentrations of NPs. For low and high control, the cells were cultured in a medium. After 48 h, 100 μL of Triton X-100 solution was inserted into high-control wells and mixed properly to ensure the destruction of the cell membranes. Afterward, the plates were centrifuged (10 min at 250 g), and the 100 μL of supernatants were transferred to another flat-bottom plate. In the next step, 100 μL of LDH mixed detection kit reagent was inserted into each well and incubated at room temperature for 30 min. The absorbance was determined using an ELISA reader at 490 nm. The cytotoxicity percentage was defined as:

$$\text{Cytotoxicity } (\%) = \frac{\text{experimental value} - \text{low control}}{\text{high control} - \text{low control}} \times 100 \tag{2}$$

2.2.5. Hemolysis assays

Fresh human blood containing appropriate anticoagulants was used for hemocompatibility tests. Various concentrations of NPs (6.25, 12.5, 25, 50, and 100 μg/ml in sterile saline solution) were prepared, and 200 μl of blood-containing anticoagulant was added to each sample. Then, the samples were kept for 1 h in an incubator with a temperature of 37 °C. The samples were centrifuged at 1500×g for 10 min. By transferring the supernatant to a 96-well plate, the absorbance of the sample was measured at a wavelength of 545 nm using a microplate reader (Biochrom, Berlin, Germany). Adding 200 μl of blood containing anticoagulant to 4 ml of distilled water was used as a positive control. Adding 200 μl of blood containing anticoagulant to normal saline was used as a negative control [26]. The percentage of hemolysis was calculated according to equation (3) and based on the absorption rate of the samples (Ds), positive control (Dpc), and negative control (Dnc).

$$\text{Hemolysis } \% = \frac{\text{Ds} - \text{Dnc}}{\text{Dpc} - \text{Dnc}} \times 100 \tag{3}$$

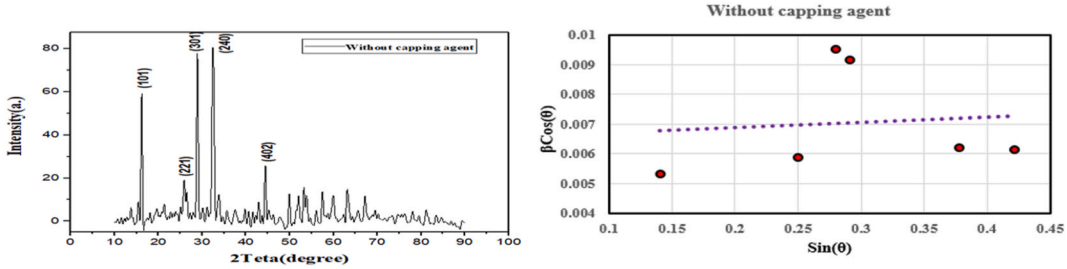

Fig. 1. X-Ray pattern of KTP NPs synthesized without capping agent.

2.3. Statistical analysis

Three repetitions were used for each experiment, and finally, the average data was calculated. Statistical tests such as one-way ANOVA, *t*-test, and Tukey's post hoc were used. $P \leq 0.05$ was considered significant.

3. Results and discussions

3.1. The powder X-Ray diffraction

Figs. 1 and 2 show the XRD patterns and William-son curves of KTP NPs synthesized without (Fig. 1) and with oxalic acid (Fig. 2.a to Fig. 2.c) and glycine (Fig. 2.d to Fig. 2.f) as capping agents with different mole ratios (after calcination at 700 °C for 2h).

X-ray diffraction spectra for all the samples confirm the formation of KTP nanocrystals with an orthorhombic phase. The average crystallite size of produced powders was calculated using William-Son-Hall [27] (Equation (4)) and Debye-Scherer (Equation (5)) methods by measuring the XRD peaks broadening and are documented in Table 1:

$$D = \frac{K\lambda}{\beta \cos(\theta)} \tag{4}$$

$$\beta \cos(\theta) = 4\varepsilon \sin(\theta) \tag{5}$$

With an increase in the mole ratio of glycine as a capping agent, the grain size of obtained NPs decreased, and their lattice strain increased. Scherer and Williamson's equations confirm these results. Glycine is an amino acid with an isoelectric point equal to pH = 6, So well-coating the nuclei is expected at this pH. Small molecules of glycine at low concentrations can't completely coat the primary nuclei. So, the glycine molecules attached to the nuclei surface increase the surface energy, growth rate, and grain size. Higher concentrations of glycine resulted in the formation of amphoteric chains of glycine molecules at pH = 6. So, well-coating the nuclei surface and smallest grain size were obtained with a 1:1 mol ratio of glycine. Using glycine as a capping agent resulted in crystal lattice rotation.

It is observed that (Table 1) and it is observed that with an increase in the oxalic acid mole ratio, the grain size of obtained NPs decreased. Maximum lattice strain was observed at a 1:2 mol ratio of oxalic acid. Oxalic is a carboxylic acid (due to its resonance bonds and small size) that has a bio-conjugation role between primary nuclei and can produce well-coated nuclei. The KTP NPs' surfaces are functionalized by carboxyl groups using oxalic acid as a capping agent. Carboxyl groups act as electron donors and coordinate with Ti ions. So, with an increase in the oxalic acid concentration, nuclei surface coating is improved, and the grain size decreases. The 1:1 mol ratio of oxalic acid resulted in crystal lattice rotation.

3.2. Fourier transform infrared spectroscopy

Fig. 3 and Table 2 shows the FTIR spectra of synthesized NPs without (Fig. 3.a) and with different mole ratios of capping agents (Fig. 3.b to Fig. 3.f) after calcination at 700 °C for 2h. The appeared peaks in the wavelength range from 1200 to 600 cm^{-1} are assigned to characteristic bonds of the KTP structure. The asymmetric stretching vibrations of PO_4 units are revealed at 974, 995, 1027, 1050, 1100, and 1126 cm^{-1} [28]. The appeared peaks at 820, 785, and 712 cm^{-1} are associated with Ti-O vibrations of the TiO_6 octahedral. The splitting of degenerate and PO_4 modes reveal in the wavenumber range from 660 to 350 cm^{-1} [29]. The formation of the KTP structure was confirmed for all samples.

The best structure with the lowest impurity absorption among obtained KTP NPs using oxalic acid as a capping agent belongs to the 1:1 mol ratio. Impurity peaks in the range of 1398–1405 cm^{-1} were assigned to C–O–H bending vibration bonds [30], which are not completely removed by heat treatment. The most absorption of C–O–H bending vibration bonds was observed using a 1:2 mol ratio of oxalic acid. Impurity peaks in the range of 1623–1645 cm^{-1} wavenumber indicate PO_4 tetrahedral and TiO_6 octahedral coordinated to C=C stretching bond. The broadest impurity peak belongs to the absorbed O-H stretching bond on the surface of synthesized NPs and was observed using a 1:2 mol ratio of oxalic. The absorption peaks in the range of 3152–3430 cm^{-1} are indicated to be O-H stretching bonds.

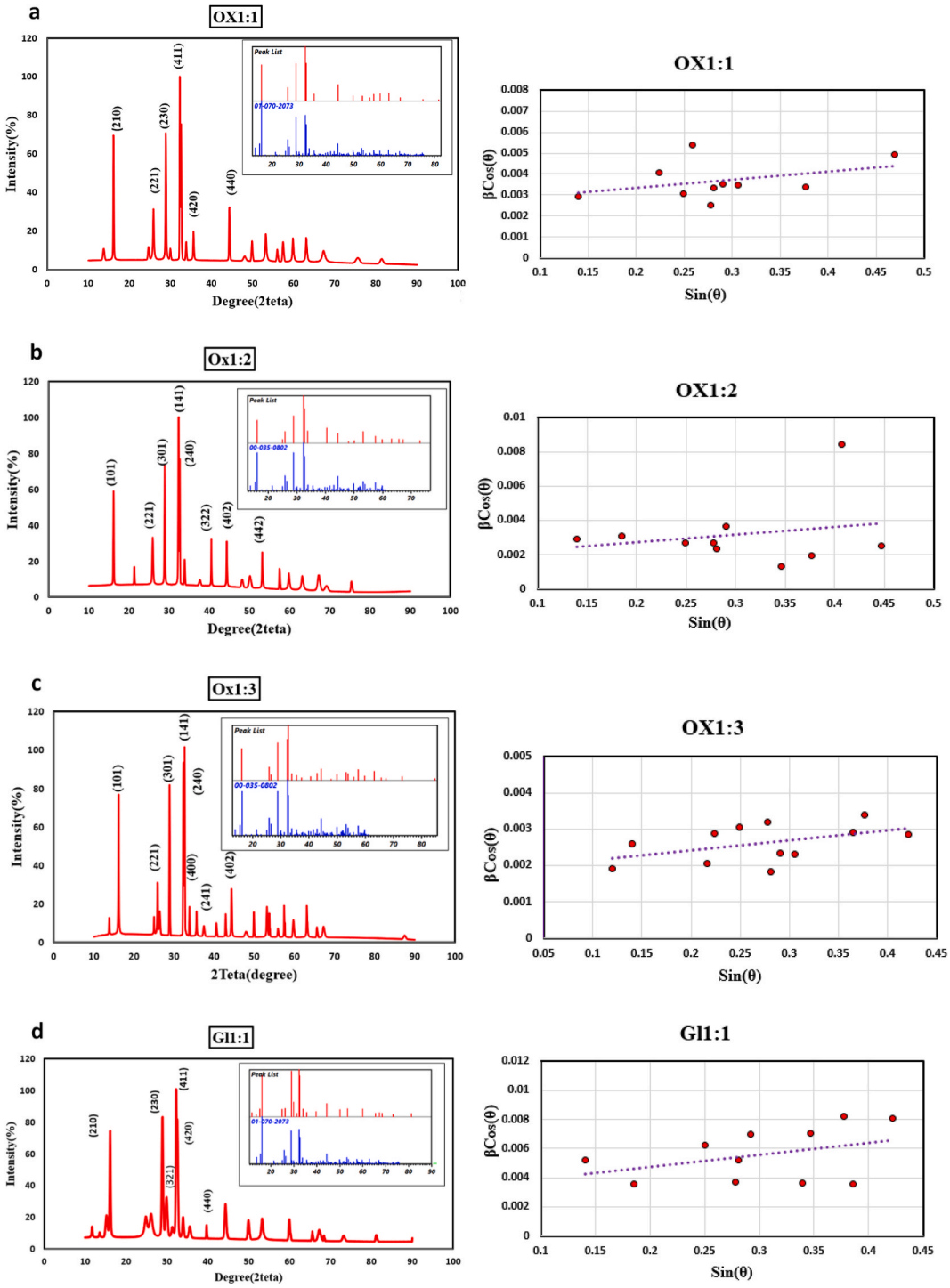

Fig. 2. X-Ray pattern of KTP NPs synthesized using oxalic acid as capping agent with (a)1:1, (b)1:2, (c)1:3 mol ratios and glycine as capping agent with (d)1:1, (e)1:2 and (f)1:3 mol ratios.

The obtained NPs using glycine as a capping agent showed the impurities peaks in the region of 1398–1405 cm^{-1} wavenumbers, which belong to carbonyl (C=O) stretching bonds of amino acids left over on the NPs surfaces after calcination. The carbonyl group is coordinated to the Ti^{2+} ions resulting in impurity peaks at 1645 cm^{-1}. The shift in carbonyl frequency reveals the interaction of KTP

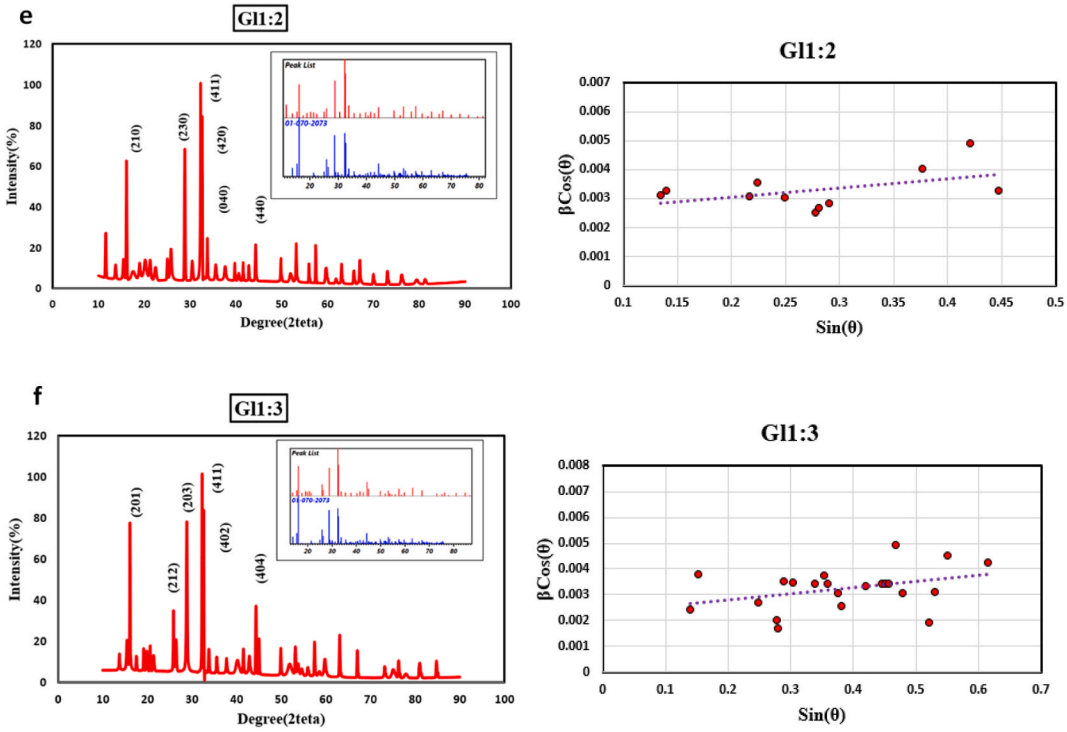

Fig. 2. (*continued*).

NPs with glycine through the carboxylic side [8]. Obtained KTP NPs using 1:1 and 1:2 mol ratios of glycine showed a strong impurity peak at 1638, which indicates N-H bonding out of the plane.

The broad absorption peaks in the range of 3167–3460 cm^{-1} indicate the absorbed O–H and N–H stretching bond on the surface of synthesized NPs [30]. The strongest impurity absorption peaks in the region of 3167–3460 cm^{-1}, 1630-1645 cm^{-1}, and 1398-1405 cm^{-1} belong to obtained KTP NPs using 1:1, 1:3, and 1:1 mol ratios of glycine, respectively.

Comparing recorded spectra of obtained KTP NPs using oxalic acid and glycine with similar concentrations are given in Fig. 3.d to Fig. 3.f. It is observed that using glycine as a capping agent results in more impurity absorption in obtained NPs.

The characteristic bonds of the KTP structure are observed for obtained NPs Using a 1:2 mol ratio of capping agents. However, the 1:1 and 1:3 mol ratios of glycine as a capping agent resulted in the weakening of the characteristic peaks. Obtained NPs using oxalic acid showed a better structure rather than synthesized NPs using glycine as a capping agent.

3.3. Raman spectroscopy

Fig. 4 shows the Raman spectra of synthesized NPs using different mole ratios of capping agents (Fig. 4.a to Fig. 4.f) after calcination at 700 °C for 2h. The vibrations of PO_4 group are symmetric stretching vibration $\upsilon_1 = 938\ cm^{-1}$, symmetric deformation $\upsilon_2 = 420\ cm^{-1}$, antisymmetric stretching vibration $\upsilon 3 = 1020$ and antisymmetric deformation vibration $\upsilon 4 = 567\ cm^{-1}$. All the fundamentals are Raman active but only υ_3 and υ_4 are active in the IR.The weak Raman lines at 536, 565, and 576 cm^{-1} in Raman spectra are assigned to the symmetric bending mode $\upsilon 2$.

Observed peaks at 798 cm^{-1} are assigned to the $\upsilon 3$ asymmetric stretching mode. The Very strong band appears at 698 cm^{-1} with the weak band at 747 cm^{-1} (Raman) are due to TiO_6 group. Very weak bands observed around 480 and 493cm^{-1} and the asymmetric bending mode $\upsilon 5$ frequencies occur at 384-330cm^{-1} in Raman attributed to the $\upsilon 4$ asymmetric bending mode of the TiO_6 group. The Raman and IR inactive asymmetric bending mode $\upsilon 6$ is observed as very intense in the Raman spectrum at 210 and 267 cm^{-1}.

The vibrational lines observed at 170 and 190 cm^{-1} with weak lines observed around 70,82,107,119,130,138 and 152cm^{-1}(Raman spectra) are assigned as external vibrational modes. The formation of the $KTiOPO_4$ structure was confirmed for all samples.

3.4. UV–Vis transmission spectroscopy

Fig. 5 shows UV–Vis spectra of KTP NPs synthesized using glycine (Fig. 5.a) and oxalic acid (Fig. 5.b) as capping agents with different concentrations. Comparing UV–Vis spectra of obtained NPs using different capping agents with similar concentrations are given in Fig. 6.

The band gap energy of obtained KTP NPs was calculated by the following equation [31]:

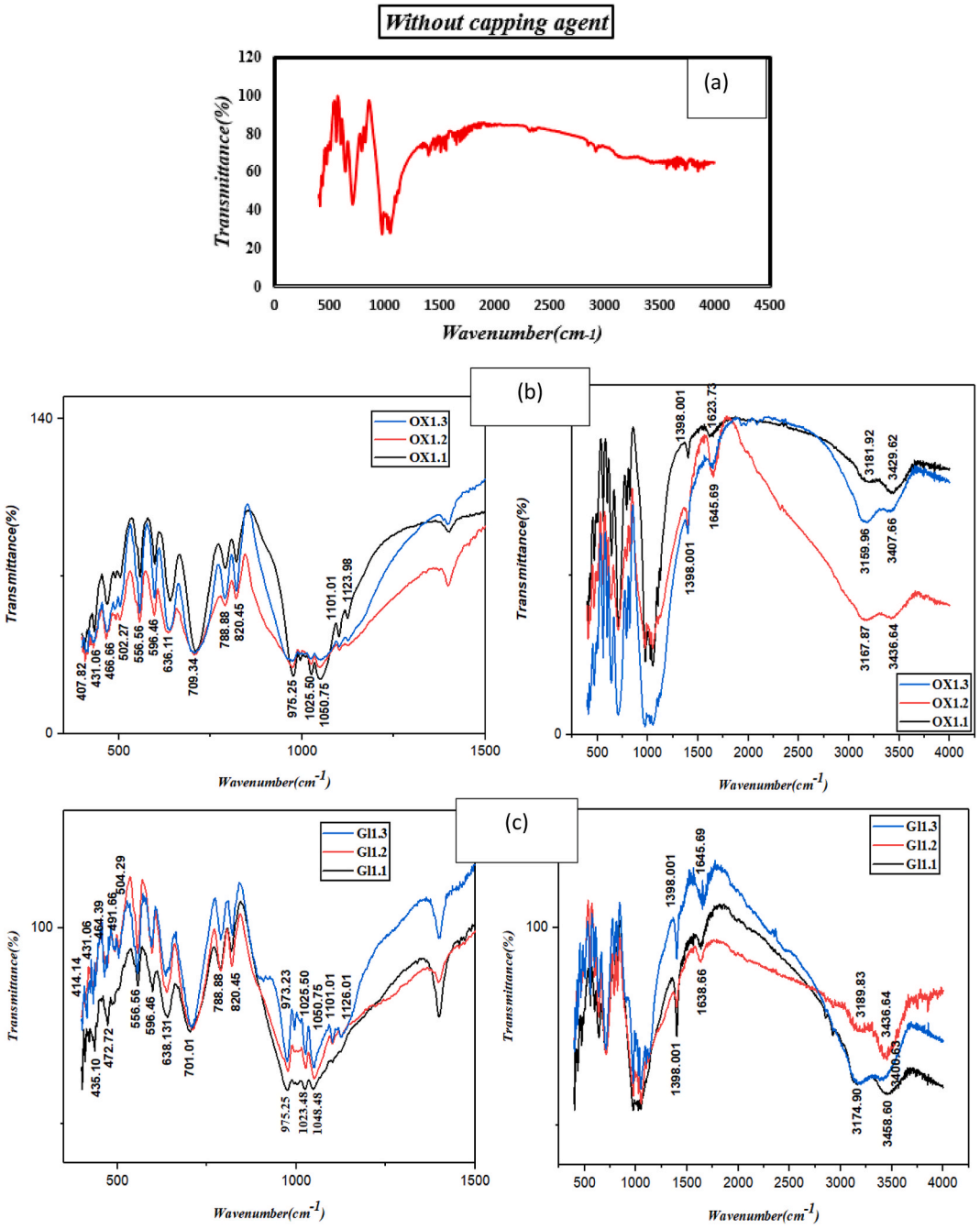

Fig. 3. FT-IR spectra of samples synthesized (a) without capping agent, (b) using oxalic acid with different mole ratios, (c) using glycine with different mole ratios, (d–f) comparing curves of obtained NPs using different capping agent with similar concentration.

$$E_g(eV) = \frac{hC}{\lambda_{onset}} \simeq \frac{1241}{\lambda_{onset}(nm)} \quad (6)$$

λ_{onset} is calculated from extrapolation of the absorption edge to the wavelength axis. For KTP NPs synthesized using different solution concentrations, the cut-off wavelengths and band gaps energy, are given in Table 3.

The highest transparency percent among obtained KTP NPs belongs to the 1:3 mol ratio of oxalic acid. Calculated band gaps from recorded UV–Vis spectra confirm a decrease in the grain size with an increase in the capping agent concentration. Only the calculated band gap of the OX1:2 sample does not follow XRD results. We guess the C=C stretching bond coordinated to PO_4 tetrahedral and TiO_6

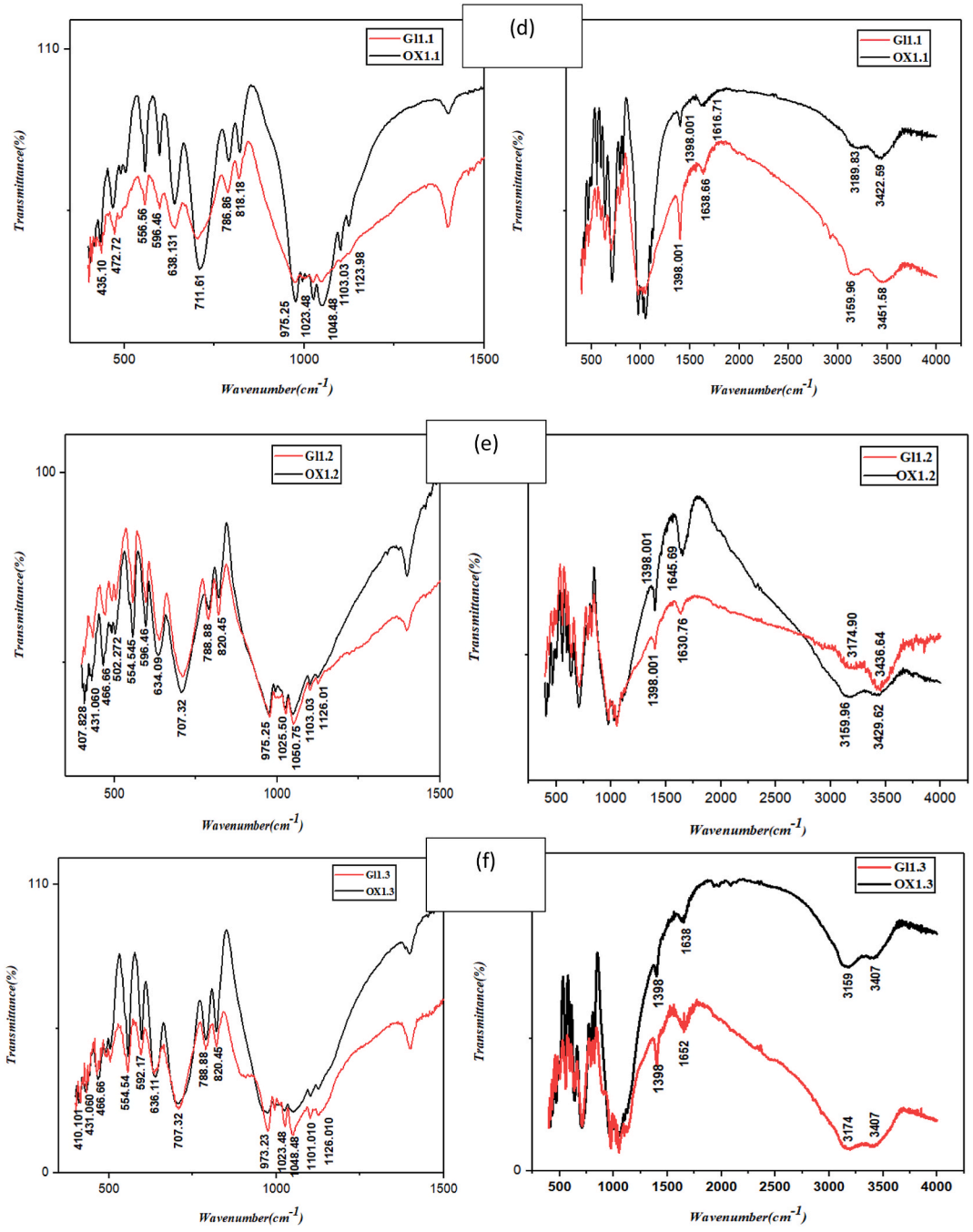

Fig. 3. (*continued*).

octahedral that is observed as strong impurity peaks in recorded UV–Vis and FT-IR spectra results in energy band gap displacement.

UV–Vis comparing spectra showed using oxalic acid as a capping agent (except 1:2 mol ratio) resulted in obtained KTP NPs with better optical quality rather than using glycine.

3.5. Scanning electron microscopy (SEM) study

Fig. 7 shows the FESEM images with accompaniment size distribution curves of KTP NPs synthesized using oxalic acid (Fig. 7.b to Fig. 7.d) and glycine (Fig. 7.e to Fig. 7.g) as capping agents with different mole ratios. Size distribution for all samples was calculated using Image-J software. Poly disparity index (PDI) was calculated via Image-J software using the following equations [32] and are

Table 2
The FTIR maxima in KTP NPs.

Chemical bond	Maximum peaks (cm^{-1})
asymmetric stretching vibrations of PO_4	974,995, 1027, 1050, 1100, and 1126
Ti-O vibrations of the TiO_6 octahedral	820, 785, and 712
splitting of degenerate and PO_4 modes	660–350
C–O–H bending vibration bonds	1398–1405
C=C stretching bond	1623–1645
O-H stretching bonds	3152–3430
carbonyl (C=O) stretching bonds	1398–1405
N-H bonding	1638
O–H and N–H stretching bond	3167–3460

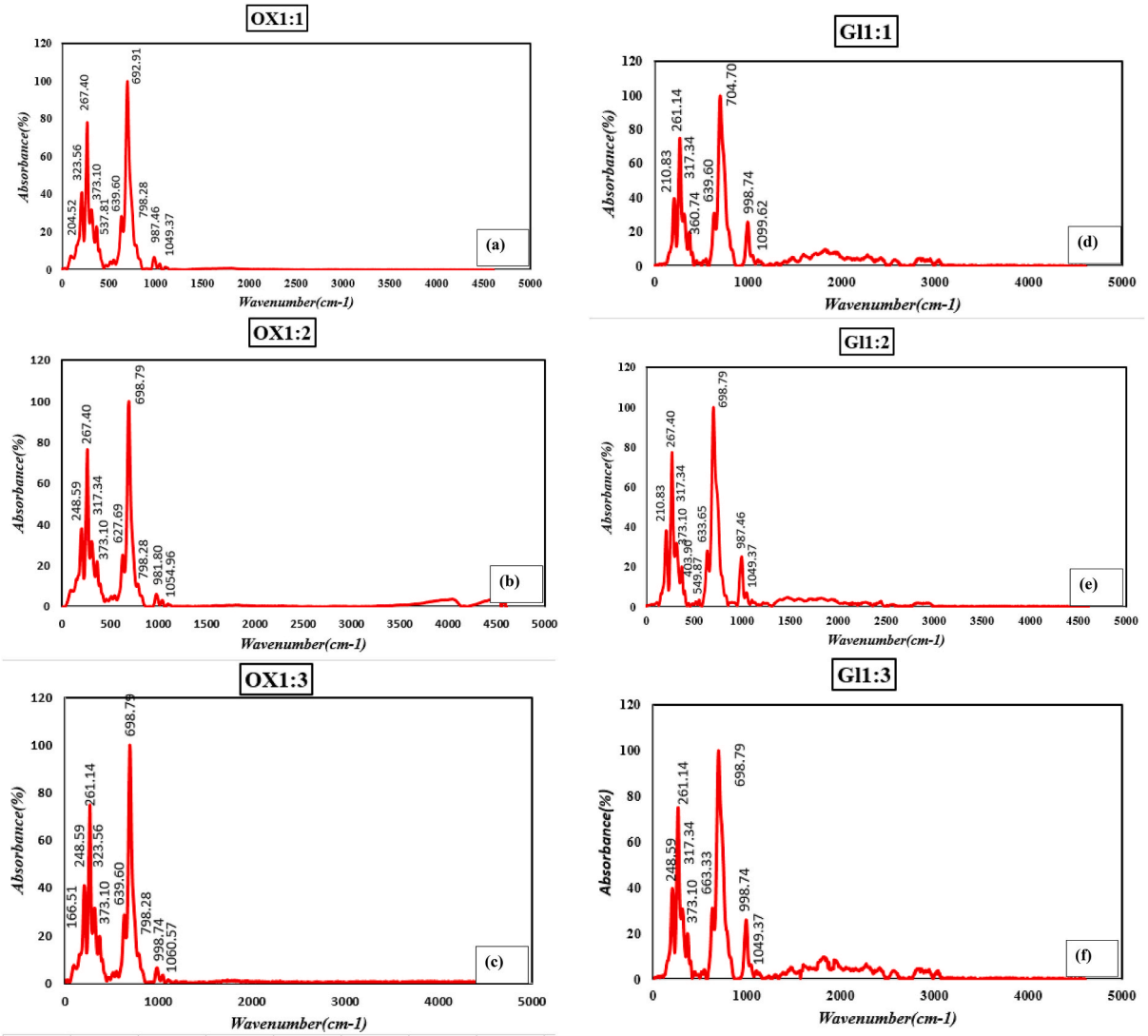

Fig. 4. Raman spectra of samples synthesized (a–c) using oxalic acid with different mole ratios, (d–e) using glycine with different mole ratios.

given in Table 1.

$$D_n = \frac{\Sigma d_i}{n} \tag{7}$$

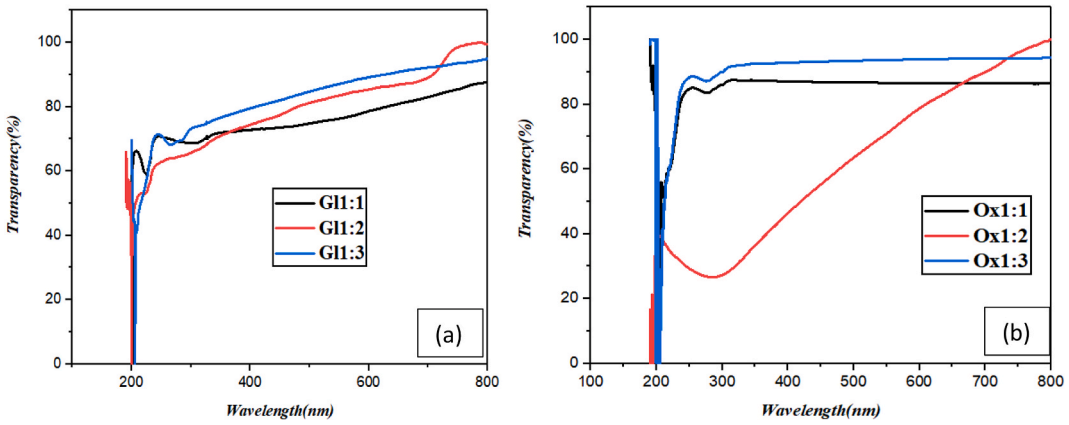

Fig. 5. UV–Vis transparency curves of samples synthesized (a) using glycine with different mole ratios, (b) using oxalic acid with different mole ratios.

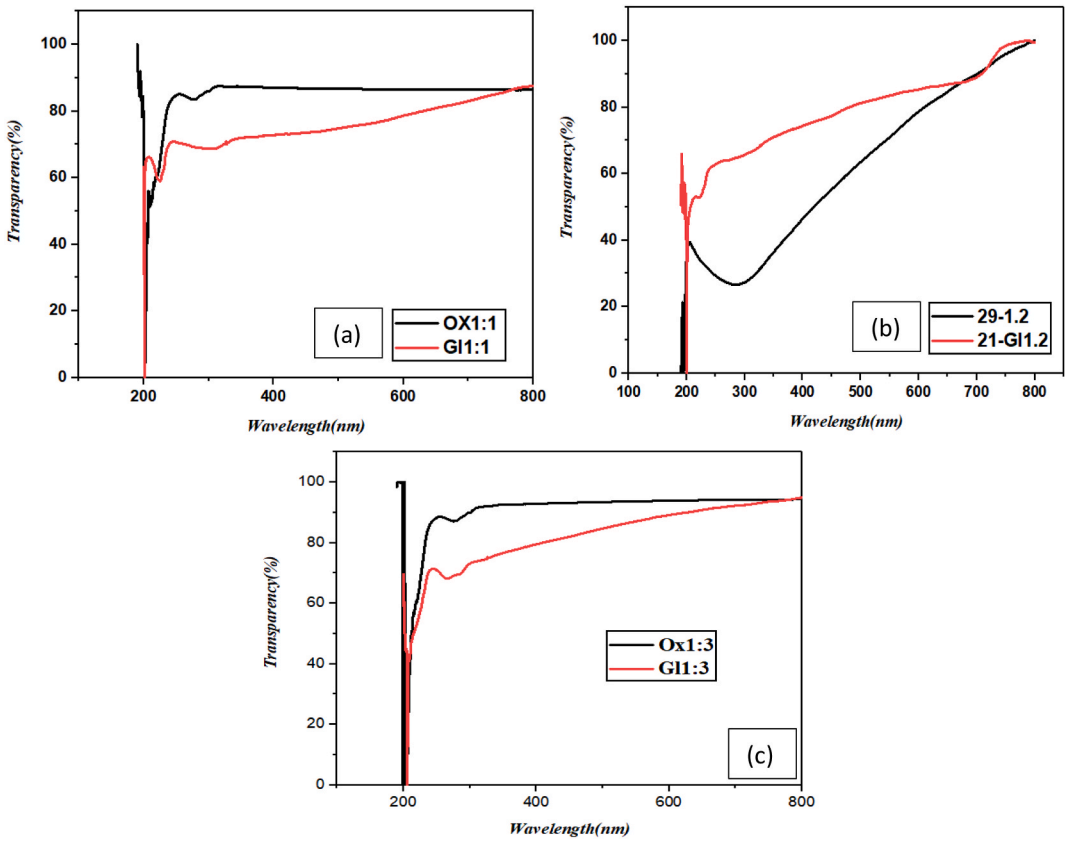

Fig. 6. Comparing UV–Vis transparency curves of obtained NPs using different capping agent with similar concentrations.

Table 3
Optical properties of obtained KTP NPs using oxalic acid and glycine as capping agents

Sample	Cut off wavelength (nm)	Band gap energy (eV)	Transparency (%) (in the wavelength region of 400-800nm)
Gl1:1	200.034	6.203	73-87
Gl1:2	201.82	6.149	72-98
Gl1:3	206.09	6.021	79-94
OX1:1	201.76	6.150	87
OX1:2	200.13	6.200	43-98
OX1:3	201.93	6.145	94

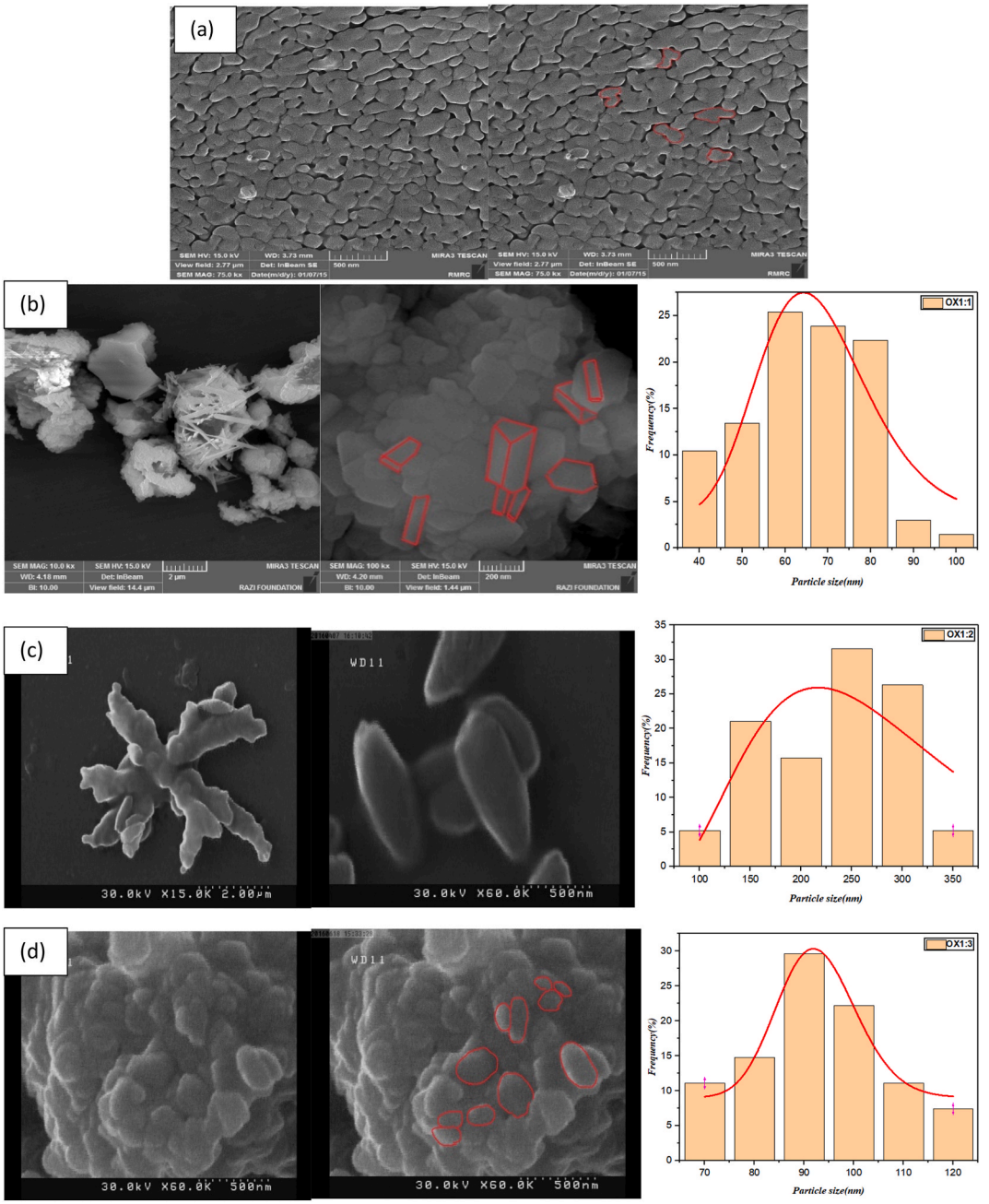

Fig. 7. FESEM images of KTP NPs synthesized (a) without capping agent, (b–d) using oxalic acid, (e–g) using glycine as capping agent with different mole ratios.

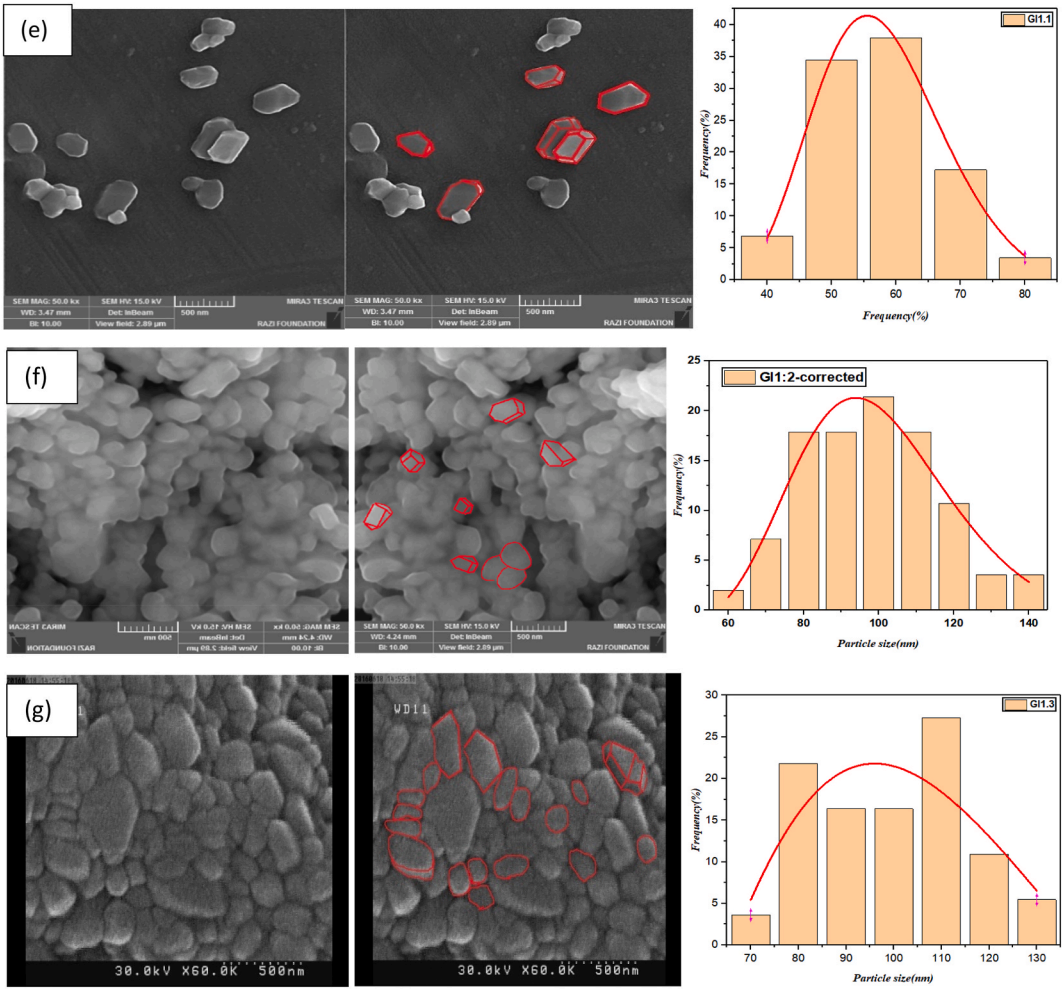

Fig. 7. (*continued*).

$$D_w = \frac{\Sigma(d_1)^4}{\Sigma(d_i)^3} \tag{8}$$

$$PDI = \frac{D_w}{D_n} \tag{9}$$

Where d_i represents the diameters of particles and n is the number of particles.

Fig. 7.a shows KTP NPs synthesized without a capping agent. It is observed that dumbbell-shaped KTP NPs with an average particle size of about 100 nm were formed.

The morphology of obtained NPs using a 1:1 mol ratio of oxalic acid is shown in Fig. 7.b. The combination of NPs with polyhedral-form (with some hundred nanometers in dimensions) and needle-type (with some hundred nanometers in diameter and micro length) are observed. Binary acid absorption on the special crystal faces promotes growth in a particular direction. Oxalic acid has a bio-conjugation role between primary nuclei due to resonance bonds and small size. So, the surface of KTP NPs was functionalized by carboxyl groups. Carboxyl groups act as electron donors and coordinate with Ti ions. Fig. 7.b shows the 1:1 mol ratio of oxalic acid is not sufficient for the oriented growth of all the primary nuclei. Therefore, only some needle-type NPs were formed, and in others, carboxyl groups resulted in size control of NPs. In this case, carboxyl groups attached to the nuclei surface can stabilize the surface energy and develop crystal faces. The observed morphology was very similar to the KTP single crystals grown by the flux method. At a 1:2 mol ratio of oxalic acid, obtained NPs showed a combination of flower-type and oval-form with 700–800 nm in length and 200–300 nm in diameter.

At a 1:3 mol ratio of oxalic acid, because of the very low concentration of the capping agent, carboxyl groups cannot completely functionalize the nuclei surface, so KTP NPs with irregular shapes were formed. The most non-uniform and the most uniform size distribution among obtained KTP NPs using oxalic acid belong to OX1:3 (PDI = 1.23) and OX1:2 (PDI = 1.11) samples.

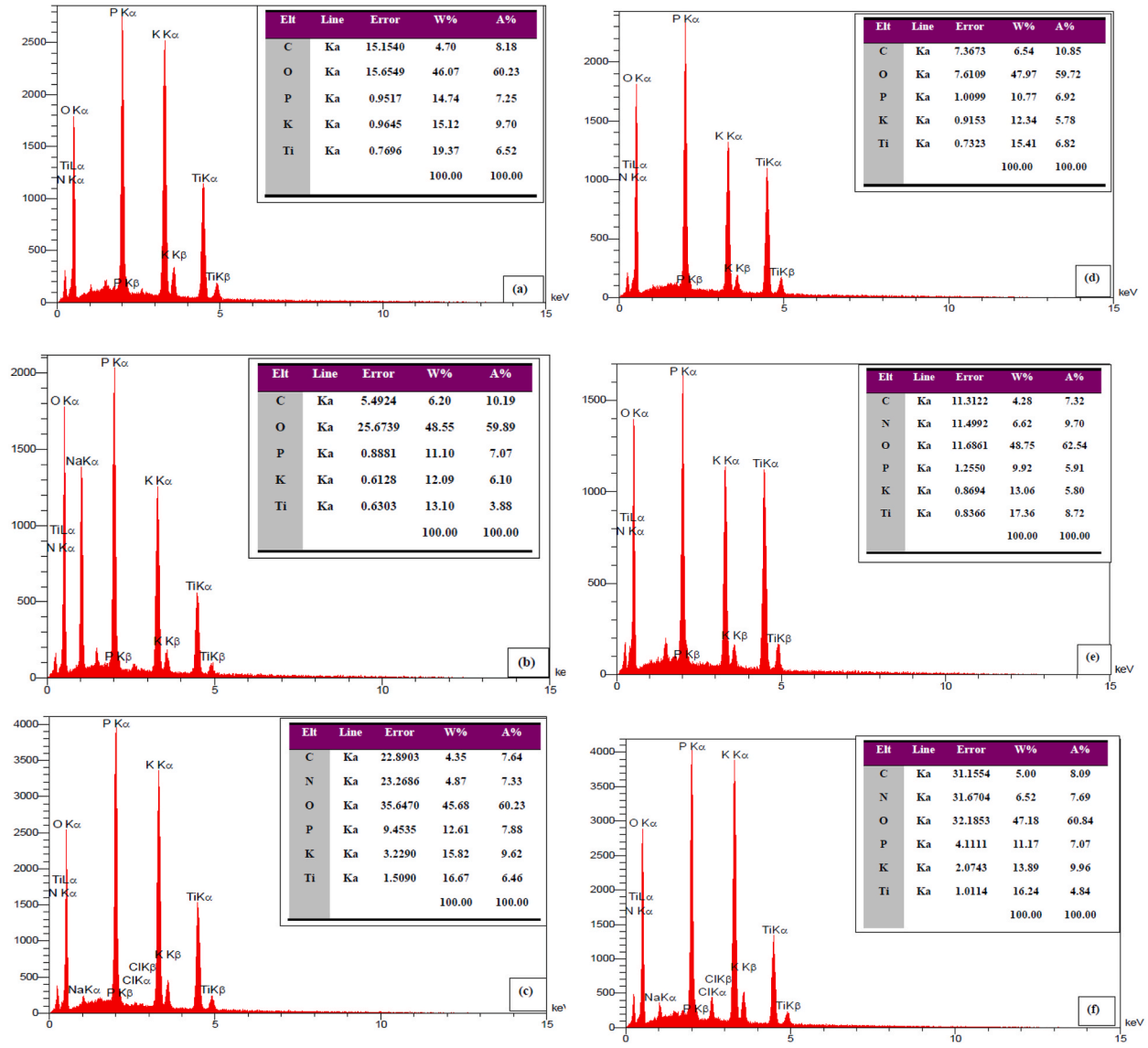

Fig. 8. EDX spectra of KTP NPs synthesized using oxalic acid as capping agent with (a)1:1, (b)1:2, (c)1:3 mol ratios and glycine as capping agent with (d)1:1, (e)1:2, and (f)1:3 mol ratios.

Fig. 6.e shows the polygonal tablet form of obtained KTP NPs using a 1:1 mol ratio of glycine as a capping agent. The favorite morphology using glycine as a capping agent in the solution-based synthesis methods is nanosheet-form. At this concentration measured average particle size was 55 nm. The small molecules of glycine are polar and hydrophilic. Glycine molecules can be placed close together on surfaces of nuclei at pH = 6 and. This pH is the iso-electric point of the glycine amphoteric molecules. So, the glycine molecules can be attached as molecule chains and coat the surface of NPs. At a 1:1 mol ratio of glycine, the complete coating of nuclei results in a decrease in the particle size of obtained KTP NPs. This concentration showed the most uniform particle size distribution.

The varied concentrations of glycine affect the morphology of KTP NPs [8]. A 1:2 mol ratio of glycine results in cubic and polyhedral forms of NPs. The average particle size at this mole ratio was 95 nm. A1:2 mol ratio of glycine was not sufficient to stabilize the nuclei surface and resulted in the formation of kinks on the nuclei surface. So, nucleation growth was done in 3 dimensions. These results are in according with other researchers' reports [22].

NPs synthesized using a 1:3 ratio of glycine as a capping agent show irregular shapes with an average particle size equal to 110 nm. These NPs showed the most non-uniform size distribution among NPs synthesized using glycine as a capping agent.

A 1:3 mol ratio of glycine and oxalic acid as a capping agent resulted in the most non-uniform size distribution among the obtained NPs. The most uniform size distribution was obtained using a 1:1 mol ratio of glycine as a capping agent. The biggest and smallest particle sizes were obtained using 1:2 and 1:1 mol ratios of oxalic acid and glycine, respectively.

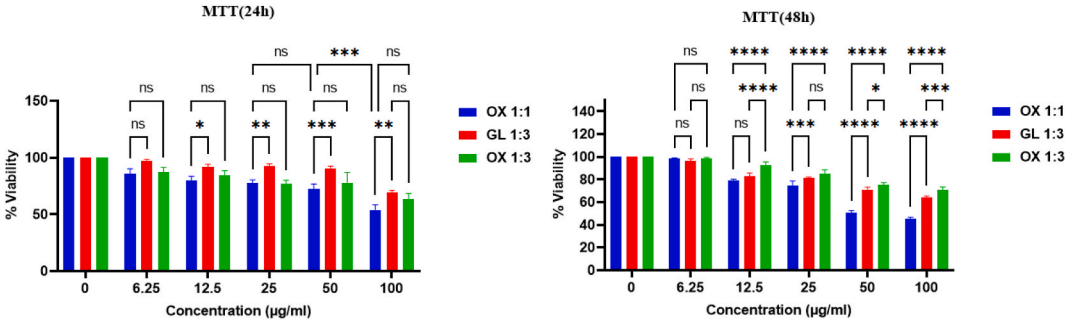

Fig. 9. Cell viabilities of the human LAN-5 neuroblastoma cell exposed to different concentrations of KTP NPs after 24h and 48h (mean ± standard deviation, p*<0.01, p**<0.001, and p****<0.0001).

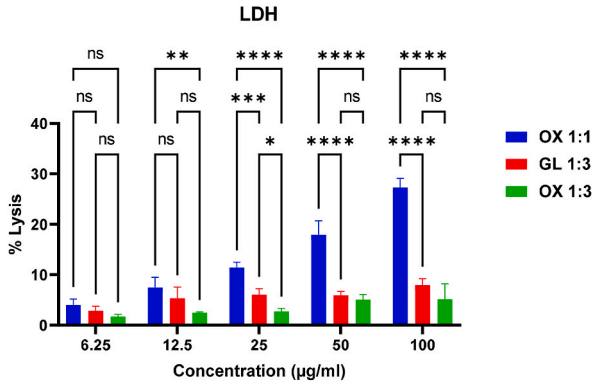

Fig. 10. The lactate dehydrogenase percent of the human LAN-5 neuroblastoma cell exposed to different concentrations of KTP (mean ± standard deviation, p*<0.01, p**<0.001, and p****<0.0001).

3.6. Energy-dispersive X-ray analysis (EDX)

Energy-dispersive X-ray spectra of obtained NPs using capping agents are given in Fig. 8(a–f).

The weight percent of elements confirms the formation of the KTP structure. Elements with an atomic number below 11 are hard to be detected using EDX. With attention to the total weight percent given in Fig. 8, we guess extra oxygen and carbon elements in Fig. 8 (a–c) belong to absorbed O_H, C–O–H, and C=C groups on the surface of nanoparticles while hydrogen elements couldn't be detected using EDX analysis. Extra oxygen, carbon, and nitrogen elements in Fig. 8(d–f) belong to carbonyl (C=O), O–H, and N–H stretching bonds on the surface of synthesized NPs using glycine as a capping agent.

3.7. Biocompatibility

MTT and LDH analyses were used to evaluate the biocompatibility of KTP NPs. The cells were exposed to various concentrations of NPs (6.25, 12.5, 25, 50, and 100 µg/ml), and their cytotoxic effects were evaluated after 24h and 48h. The results are given in Figs. 9 and 10.

Fig. 9 shows that the biocompatibility was decreased with increasing the KTP NPs concentration. Among all samples, the obtained NPs using a 1:3 mol ratio of glycine show the best biocompatibility after 24h. The lowest concentration of obtained NPs using a 1:1 mol ratio of oxalic acid showed good biocompatibility, but the cell viability strongly decreased with an increase in their concentration. Obtained NPs using a 1:3 mol ratio of oxalic acid showed the best biocompatibility after 48h. Similar to the previous time point (24h) obtained KTP NPs using a 1:1 mol ratio of oxalic acid showed the best biocompatibility at the lowest concentration. However, with an increase in the concentrations, this value strongly decreased. The level of lactate dehydrogenase (LDH) was studied for different concentrations of KTP NPs (Fig. 10). Obtained KTP NPs using a 1:1 mol ratio of oxalic acid resulted in the highest cytotoxicity and damaged cells. The lowest ones were observed for obtained NPs using a 1:3 mol ratio of oxalic acid. The biocompatibility of NPs is highly dependent on their shape, size, and composition [33,34]. We guess the needle-form of obtained NPs using a 1:1 mol ratio of oxalic acid resulted in a strongly decreased biocompatibility and increased cell cytotoxicity at higher NPs concentrations. The results of the LDH test confirm it.

The preparation, surface modifications and functionalization, surface chemistry, and chemically reactive sites [35] of KTP NPs, determine the amount of NPs' biocompatibility. The surface modification of the NPs by forming a bioactive ligand affects the

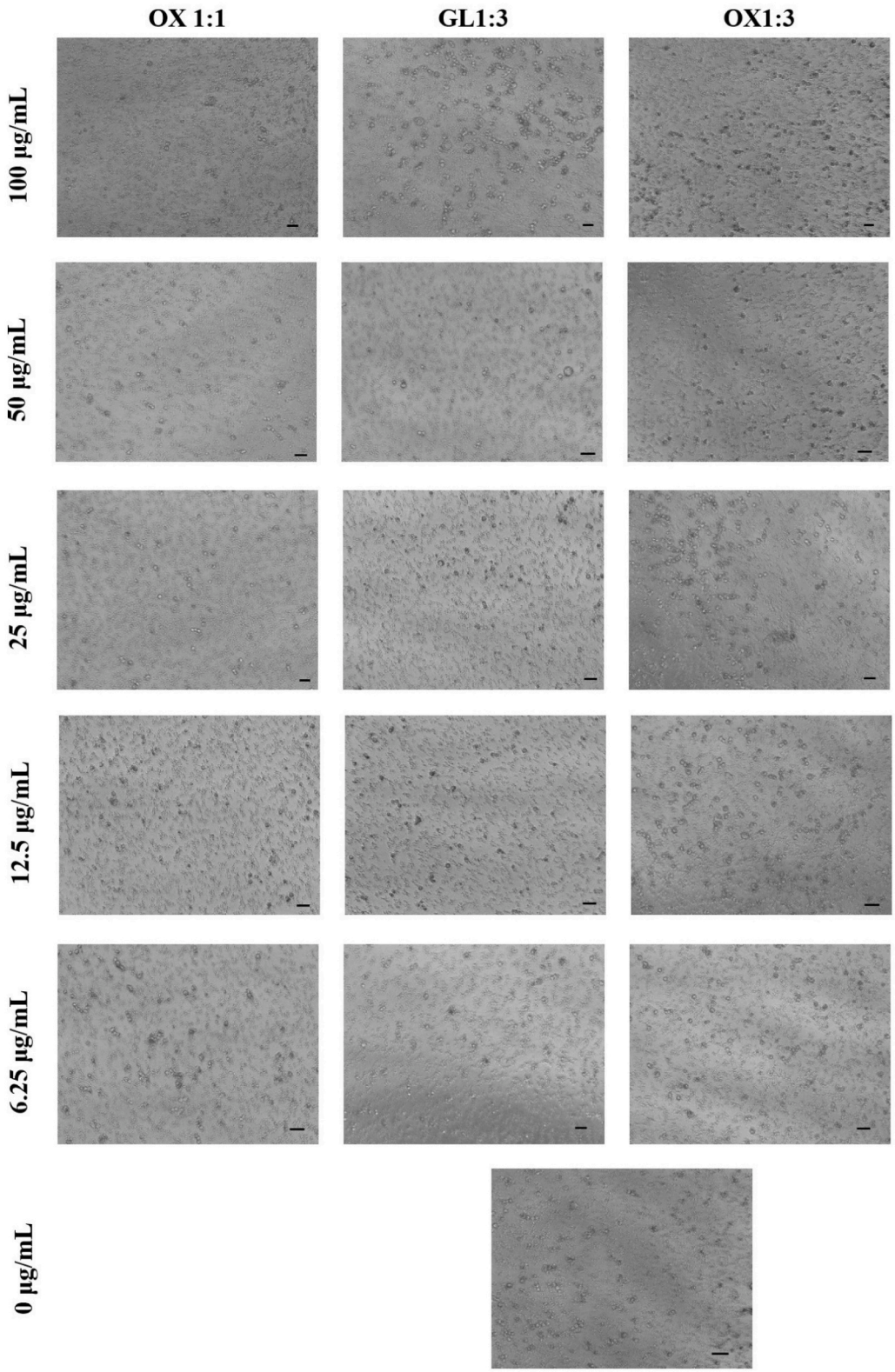

Fig. 11. LAN-5 cell morphology in different groups after 24h exposure to KTP NPs (Scale bar:50 µm).

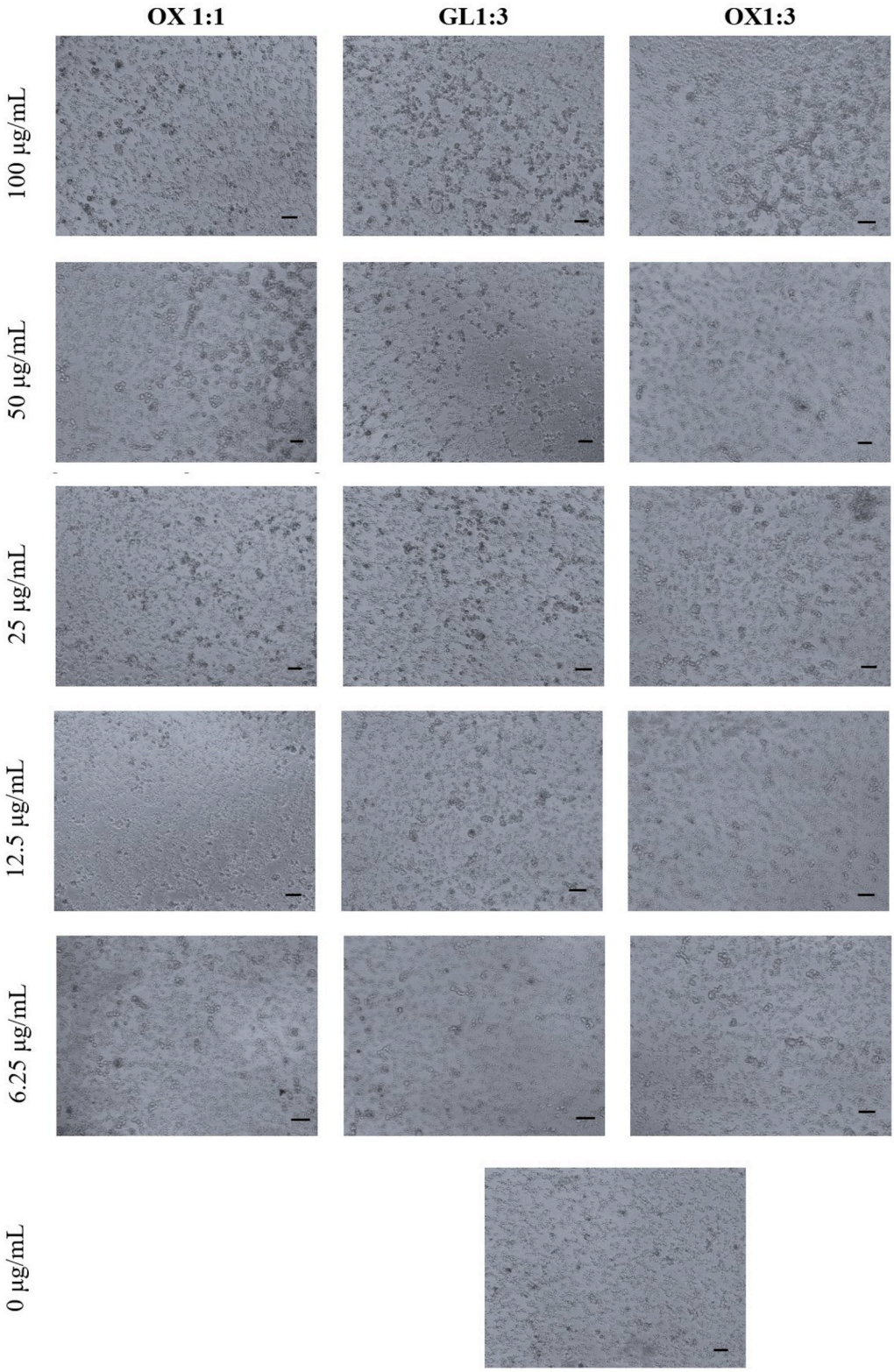

Fig. 12. LAN-5 cell morphology in different groups after 48h exposure to KTP NPs (Scale bar:50 µm).

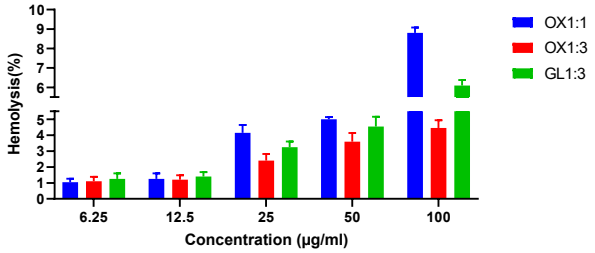

Fig. 13. Hemolysis percentages of KTP NPs.

enhancement of cell adhesion and proliferation. C–O–H bending vibration bonds and O-H stretching bond residues generated due to the thermal decomposition of oxalic acid on the surface of synthesized NPs, also carbonyl (C=O) stretching bonds of amino acids and O–H and N–H stretching bonds left over on the surface of synthesized NPs using glycine as capping agent after heat treatment was confirmed by FT-IR analysis. Surface modification of KTP NPs by mentioned bonds can alter the surface topography and chemistry, which directly affect the interaction between KTP NPs and biological environments. The formation of carbon bonding seems to be suitable to increase cellular biocompatibility [36].

The hydrophilic structures are crucial for cell adhesion, cell activity, proliferation, and biological applications [37–39]. Improved hydrophilicity and wettability of nucleation surfaces are achieved using the hydroxyl groups [34]. Hydrogen bonding can occur on the surface of NPs between free OH groups and H_2O molecules [40,41]. So hydroxyl groups left over on the surface of obtained NPs using a 1:3 mol ratio of oxalic acid and glycine are beneficial for increasing biocompatibility. After 48h, 6.25 µg/ml concentration of KTP NPs synthesized using a 1:3 mol ratio of oxalic acid showed the best biocompatibility. The images of cell morphology after exposure to different nanoparticles confirm the above results (Figs. 11 and 12).

Amine group residue on the surface of obtained NPs using a 1:3 mol ratio of glycine resulted in a decrease in their biocompatibility after 24h. The time-dependent reaction between amino groups and the biocompatibility environment has been reported by researchers [21]. We guess after 24h, the extra electron of nitrogen increases the number of delocalized electrons and, therefore, increases the surface activity. On the other hand, hydrophobic amino groups showed cytotoxicity and resulted in enhanced interaction with the cell membrane. Adding amine groups to hydroxyl groups [41] on the surface of NPs increases the cytotoxicity and Biodegradability. Reports by other researchers confirm these results [20,21]. Therefore, a time duration equal to 48h showed a decrease in the biocompatibility of the Gl1:3 sample. Although glycine as an amino acid shows biocompatibility properties, amino group residue after heat treatment shows a cytotoxicity effect after 24h and results in decreasing the biocompatibility properties.

3.8. Hemolysis test

Fig. 13 shows the percentage of hemolysis of KTP NPs at different concentrations. According to the figure, all groups had a lower hemolysis percentage than the control group. The percentage of hemolysis increased with the increase in the concentration of NPs; however, it was always in the acceptable range (up to 50 µg/ml). With an extensional increase in concentration, the percentage of hemolysis corresponding to the OX 1:1 and GL 1:3 groups was a little more than 5 % (as the accepted value for blood compatibility). Therefore, concentrations less than 50 µg/ml cause less damage to red blood cells and, therefore, lead to less hemoglobin release. The needle shape of OX 1:1 NPs can be considered as an important factor for damaging the membrane of red blood cells. In addition, the relatively positive charge of glycine in the bloodstream can interact with a variety of negatively charged membrane compounds, change the polarized structure of the membrane, and lead to red blood cell membrane rupture in the GL 1:3 group, which confirms our results [42].

4. Conclusion

KTP NPs were synthesized using glycine and oxalic acid as capping agents by the co-precipitation method. The effect of the type and concentration of the capping agent on the structural, optical, and biocompatibility properties of NPs were studied.

The amount of capping agent during synthesis helps to turn and regulate the morphology, and also modify the surface chemical properties of the NPs. The smallest grain size (12.54 nm) and particle size (55 nm) and the most uniform size distribution (1.05) were obtained using the 1:1 mol ratio of glycine as a capping agent. Using oxalic acid and glycine as capping agents results in increasing the uniformity of size distribution, but a decrease in the grain size is observed only with a 1:1 mol ratio of capping agents. The presence of C–O–H bending vibration, O–H, N–H, and carbonyl (C=O) stretching bonds left over on the surface of synthesized NPs after heat treatment was confirmed by FT-IR analysis. The bond residue functionalizes the surface of the NPs. Our results showed using glycine as a capping agent is beneficial to produce KTP NPs for short-term imaging until 24h, but the amino groups result in a decreasing the biocompatibility of NPs over time. The presence of hydroxyl groups improved the biocompatibility of obtained KTP NPs using a 1:3 mol ratio of oxalic acid as a capping agent with an increase over time. We induce oxalic acid as an attractive capping agent to synthesize appropriate KTP NPs for long-term imaging. 1:1 and 1:3 mol ratios of oxalic acid resulted in synthesized NPs with the best optical quality. Using oxalic acid as a capping agent resulted in needle-type, flower-type, and oval-form NPs, polygonal tablet form, and the cubic and polyhedral forms of KTP NPs synthesized using glycine. Our research showed the needle form of obtained NPs using

a 1:1 mol ratio of oxalic acid resulted in a substantial decrease in biocompatibility and an increase in cell cytotoxicity at higher concentrations.

CRediT authorship contribution statement

Elaheh Gharibshahian: Writing – review & editing, Supervision, Project administration, Methodology, Investigation, Conceptualization. **Maliheh Gharibshahian:** Writing – original draft, Visualization, Resources, Conceptualization. **Majid Jafar Tafreshi:** Investigation, Formal analysis, Conceptualization. **Marjan Bahraminasab:** Formal analysis. **Samaneh Arab:** Formal analysis.

Declaration of competing interest

The authors declare no conflicts of interest with respect to the research, authorship, and/or publication of this article.

References

[1] B.R. Smith, S.S. Gambhir, Nanomaterials for in vivo imaging, Chem. Rev. 117 (3) (2017) 901–986.
[2] Y. Fan, et al., Hydrologic regulation of plant rooting depth, Proc. Natl. Acad. Sci. USA 114 (40) (2017) 10572–10577.
[3] L. Le Xuan, et al., Photostable second-harmonic generation from a single KTiOPO4 nanocrystal for nonlinear microscopy, Small 4 (9) (2008) 1332–1336.
[4] L. Mayer, et al., Single KTP nanocrystals as second-harmonic generation biolabels in cortical neurons, Nanoscale 5 (18) (2013) 8466–8471.
[5] L. Le Xuan, et al., KTiOPO4 single nanocrystal for second-harmonic generation microscopy, in: Nanocrystals, IntechOpen, 2010.
[6] M. Galceran, et al., Synthesis and characterization of KTiOPO4 nanocrystals and their PMMA nanocomposites, Nanotechnology 20 (3) (2008) 035705.
[7] R.N.A. Narayana Perumal, Review on gray track effects on potassium titanyl phosphate single crystals, JOJ Material Sci. 3 (3) (2017).
[8] N. Agasti, V.K. Singh, N. Kaushik, Synthesis of water soluble glycine capped silver nanoparticles and their surface selective interaction, Mater. Res. Bull. 64 (2015) 17–21.
[9] J.D. Bierlein, et al., Fabrication and characterization of optical waveguides in KTiOPO4, Appl. Phys. Lett. 50 (18) (1987) 1216–1218.
[10] S. Dahaoui, et al., Electric properties of KTiOPO4 and NaTiOPO4 from temperature-dependent X-ray diffraction, J. Appl. Crystallogr. 32 (1) (1999) 1–10.
[11] C.J. Barbé, M.A. Harmer, G.W. Scherer, Sol-gel synthesis of potassium titanyl phosphate: solution chemistry and gelation, J. Sol. Gel Sci. Technol. 9 (1997) 183–199.
[12] Y. Kanno, Synthesis and sintering of KTiOPO4, via mechanochemical mixing route, J. Alloys Compd. 210 (1–2) (1994) 45–52.
[13] N. Madari, E. Gharibshahian, M. Tafreshi, Novel synthesis of KTP nanoparticles by combustion method using urea and glycine fuels, Appl. Phys. A 128 (2022) 1–14.
[14] S.K. Biswas, A. Pathak, P. Pramanik, Synthesis of nanocrystalline ktiopo4 powder by chemical method, J. Am. Ceram. Soc. 90 (4) (2007) 1071–1076.
[15] E. Gharibshahian, M.J. Tafershi, M. Fazli, Effects of solution concentration and capping agents on the properties of potassium titanyl phosphate nanoparticles synthesized using a co-precipitation method, J. Phys. Chem. Solid. 116 (2018) 241–249.
[16] E. Gharibshahian, M.J. Tafreshi, M. Behzad, The effects of solution pH on structural, optical and electrical properties of KTiOPO4 (KTP) nanoparticles synthesized by hydrothermal method, Opt. Mater. 109 (2020) 110230.
[17] M. Houshiar, et al., Synthesis of cobalt ferrite (CoFe2O4) nanoparticles using combustion, coprecipitation, and precipitation methods: a comparison study of size, structural, and magnetic properties, J. Magn. Magn Mater. 371 (2014) 43–48.
[18] Y. Yang, et al., Optically active nanomaterials for bioimaging and targeted therapy, Front. Bioeng. Biotechnol. 7 (2019) 320.
[19] J. Yang, et al., One-step hydrothermal synthesis of carboxyl-functionalized upconversion phosphors for bioapplications, Chem.–Eur. J. 18 (43) (2012) 13642–13650.
[20] A. Pinazo, et al., Amino acids as raw material for biocompatible surfactants, Ind. Eng. Chem. Res. 50 (9) (2011) 4805–4817.
[21] O.S. Adeyemi, et al., Exploring amino acid-capped nanoparticles for selective anti-parasitic action and improved host biocompatibility, J. Biomed. Nanotechnol. 14 (5) (2018) 847–867.
[22] P. Basnet, et al., Glycine-A bio-capping agent for the bioinspired synthesis of nano-zinc oxide photocatalyst, J. Mater. Sci. Mater. Electron. 31 (2020) 2949–2966.
[23] D. Predoi, S.L. Iconaru, M.V. Predoi, Bioceramic layers with antifungal properties, Coatings 8 (8) (2018) 276.
[24] D. Predoi, et al., Zinc doped hydroxyapatite thin films prepared by sol–gel spin coating procedure, Coatings 9 (3) (2019) 156.
[25] D. Predoi, et al., Impact of gamma irradiation on the properties of magnesium-doped hydroxyapatite in chitosan matrix, Materials 15 (15) (2022) 5372.
[26] C.-H. Ooi, et al., Physicochemical evaluation and in vitro hemocompatibility study on nanoporous hydroxyapatite, J. Mater. Sci. Mater. Med. 30 (2019) 1–10.
[27] P. Bindu, S. Thomas, Estimation of lattice strain in ZnO nanoparticles: X-ray peak profile analysis, J. Theor. Appl. Phys. 8 (2014) 123–134.
[28] J. Jacco, The infrared spectra of KTiOPO4 and a K2O P2O5 TiO2 glass, Mater. Res. Bull. 21 (10) (1986) 1189–1194.
[29] C. Kannan, Investigations on the Growth of KTiOPO4 RbTiOPO4 and LiB3O5 Single Crystals and Their Electrical and Optical Characterization, 2002.
[30] J. Park, C.-S. Hwang, Differential surface capping effects on the applications of simple amino-acid-capped ZnS: Mn nanoparticles, Micromachines 12 (9) (2021) 1064.
[31] A. Rahdar, Effect of 2-mercaptoethanol as capping agent on ZnS nanoparticles: structural and optical characterization, J Nanostruct. Chem. 3 (2013) 1–5.
[32] A. Nematollahzadeh, M.J. Abdekhodaie, A. Shojaei, Submicron nanoporous polyacrylamide beads with tunable size for verapamil imprinting, J. Appl. Polym. Sci. 125 (1) (2012) 189–199.
[33] T. Mokari, M. Zhang, P. Yang, Shape, size, and assembly control of PbTe nanocrystals, J. Am. Chem. Soc. 129 (32) (2007) 9864–9865.
[34] X. Peng, et al., Shape control of CdSe nanocrystals, Nature 404 (6773) (2000) 59–61.
[35] S. Fiorito, et al., Toxicity and biocompatibility of carbon nanoparticles, J. Nanosci. Nanotechnol. 6 (3) (2006) 591–599.
[36] W.F. Xu, Biocompatibility and medical application of carbon material, Key Eng. Mater. 452 (2011) 477–480.
[37] R. Borah, et al., Surface functionalization-induced enhancement in surface properties and biocompatibility of polyaniline nanofibers, RSC Adv. 5 (60) (2015) 48971–48982.
[38] N. Jirofti, D. Mohebbi-Kalhori, R. Masoumi, Enhancing biocompatibility of PCL/PU nano-structures to control the water wettability by NaOH hydrolysis treatment for tissue engineering applications, J. Ind. Textil. 51 (2_suppl) (2022) 3278S–3296S.
[39] A. Ullah, et al., In vitro biocompatibility, antibacterial activity, and release behavior of halloysite nanotubes loaded with diclofenac sodium salt incorporated in electrospun soy protein isolate/hydroxyethyl cellulose nanofibers, Curr. Res. Biotechnol. 4 (2022) 445–458.
[40] S. Bonakdar, et al., Comparison of the Effect of Hydrophilicity on Biocompatibility and Platelet Adhesion of Two Different Kinds of Biomaterials, 2008.
[41] Q.-F. Zhang, et al., Amino acid-modified polyethylenimines with enhanced gene delivery efficiency and biocompatibility, Polymers 7 (11) (2015) 2316–2331.
[42] C. Guo, K.E. McMartin, The cytotoxicity of oxalate, metabolite of ethylene glycol, is due to calcium oxalate monohydrate formation, Toxicology 208 (3) (2005) 347–355.